



3D-QSAR Modeling and Molecular Docking Studies of novel triazoles-quinine derivatives as antimalarial agents

Ayoub Khaldan^{1,*}, Khalil El khatabi¹, Reda El-Mernissi¹, Adib Ghaleb¹, Rachid Hmamouchi¹, Abdelouahid Sbai¹, Mohammed Bouachrine^{1,2} and Tahar Lakhlifi¹

¹Molecular Chemistry and Natural Substances Laboratory, Faculty of Science, Moulay Ismail University of Meknes, Morocco

²EST Khenifra, Sultan Moulay Sliman University, Benimellal, Morocco

Received 09 Jan 2020,
Revised 06 Feb 2020,
Accepted 08 Feb 2020

Keywords

- ✓ 3D-QSAR ,
- ✓ Antimalarial,
- ✓ CoMFA,
- ✓ CoMSIA,
- ✓ Molecular docking,
- ✓ quinine- triazole.

a.sbai@umi.ac.ma ;
Phone: +212679364637

Abstract

In this study, Three-dimensional quantitative structure–activity relationship (3D-QSAR) using comparative -molecular field analysis (CoMFA) and comparative molecular similarity indices analysis (CoMSIA) models were carried out on a serie of thirty -two of novel triazoles quinine derivatives as antimalarial agents having pIC₅₀ ranging from 7.568 to 4.387 (IC₅₀ in nM). The CoMFA and CoMSIA models were employed to predict biological activity of twenty-six compounds used as training set, they give a significant coefficient of determination R² (0.98 and 0.95, respectively) as well as a high values of leave-one-out cross validation coefficient Q² (0.61 and 0.76, respectively). The predictive ability of these models was determined using a test set of 6 molecules with predicted determination coefficients Rtest² values 0.92 and 0.85 respectively. Based on these results and contour maps produced by the CoMFA and CoMSIA, we proposed new compounds with high predicted activities. Furthermore, surflex-docking carried out to confirm the stability of predicted molecules in the receptor with PDB code: 1J3K.

1. Introduction

In 2016, World Health Organization (WHO) signalized 216 million clinical cases against malaria and 445,000 deaths [1, 2].

Chinese writings first documented the apparition of malaria approximately five thousand years ago [3], half of the world's population is still a danger of contracting this destructive disease today [4]. Its broadcast results in 200 and 300 million cases in every year and an estimated 1 to 3 million malaria-related deaths yearly, most of which are pregnant women and children under the age of five years [5, 6]. Malaria is a life-threatening parasitic disease transferred by the bite of the Anopheles mosquito. There are four types of human malaria Plasmodium falciparum, Plasmodium vivax, Plasmodium ovale, and Plasmodium malaria of which the first two are the more common. The best lethal species is P. falciparum, found mainly in Africa [7].

P. falciparum gets accrued in the brain capillaries and organ defeats leading to coma and eventually decease if left untreated. There is increasing prove that the lethality of P. vivax has been miscalculated [8]. Improvements in malaria explore are frequently reviewed [2, 9, 10] and a recent monograph [11] will evidence beneficial to the medicinal chemist. This digest covers certain of the best pertinent progress in malaria drug discovery from 2010 to 2012. The loss of these reasonably priced [12] and the constant danger of resistance need for the growth of new, effective and economical antimalarial chemotherapy drugs.

The triazoles are cyclic organic compounds having a ring with five atoms, having two double bonds and 3 nitrogen atoms, therefore of formula $C_2H_3N_3$. They are aromatic and are part of the excess cycles in electrons, exhibit promising *in vivo* antimalarial activities. Further, diver's triazole-based drugs have previously used in clinics for the treatment of various diseases, demonstrating the excellent pharmaceutical profiles. Moreover, triazole derivatives can be used to fight for clinical unfolding in the control and eradication of malaria. This review covers the new developments of triazole analogues mostly triazole hybrids as potential antimalarial [13].

Recently, the development of computational chemistry directed to new successes and challenges in the drug discovery. Quantitative structure-activity relationship (QSAR) techniques along with docking methods are used to investigate the structure-activity relationship (SAR) of new compounds [14]. In this study, Comparative molecular field analysis (CoMFA) [15] and comparative molecular similarity indices analysis (CoMSIA) [16] were performed to determine regions with the ability to specific interactions (electrostatic, steric, hydrophobic, hydrogen bonds, which may increase or decrease the activity). The application of these methods gave the opportunity us to predict the activities of the molecules under study and to propose some novel triazole derivatives as antimalarial agents.

2. Material and Methods

A database of thirty-two compounds obtained from literature [17] consisted of novel triazole-quinine derivatives as antimalarial agents, the data set was split into two sets, twenty-six compounds were selected as training set and six compounds were selected as test set, relying on a random selection to evaluate the ability of the model founded. The chemical structures of both the training and test set compounds are listed in figure 1 and table 1. This data is used to build 3D-QSAR model and to examine their physicochemical properties. For the QSAR analysis the *in vitro* biological activities IC_{50} (nM) were converted into the corresponding pIC_{50} values (i.e. pIC_{50} is the negative logarithm of IC_{50} , ($pIC_{50} = -\log_{10}(IC_{50})$). 3D structure building and all modeling were employed using the Sybyl 2.0 program package.

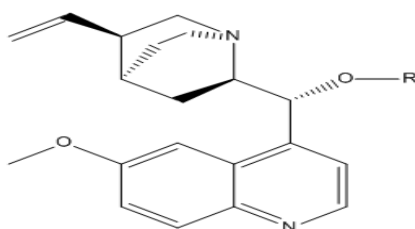
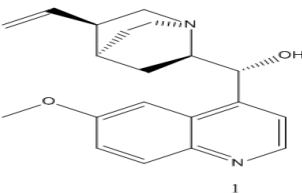
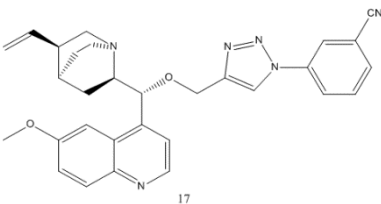
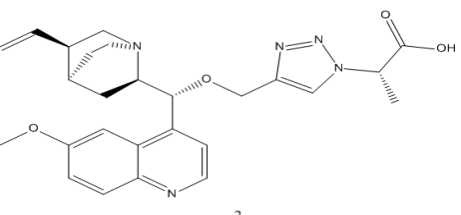
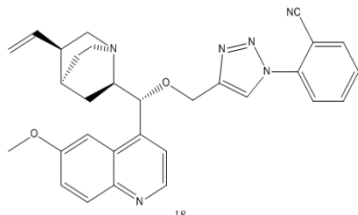
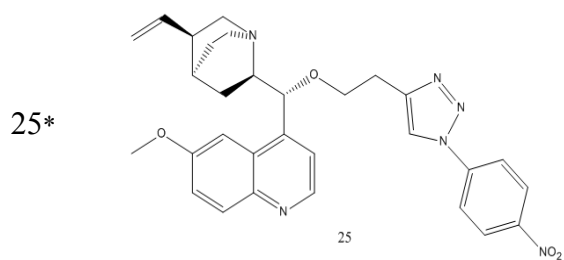
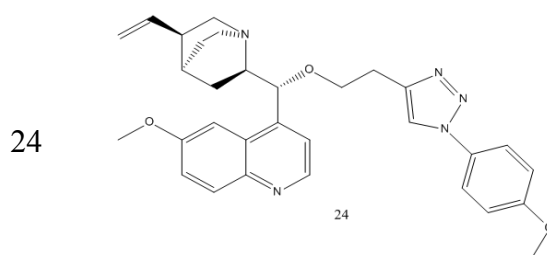
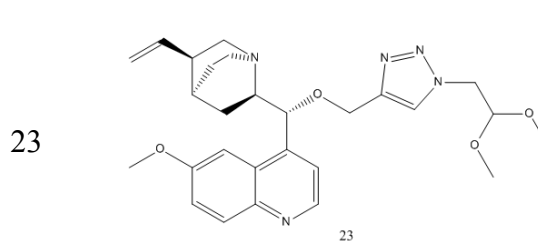
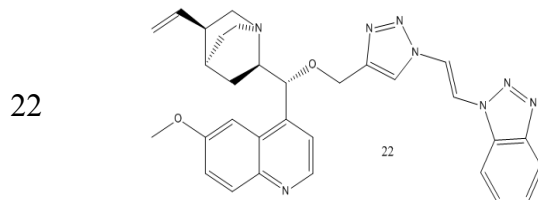
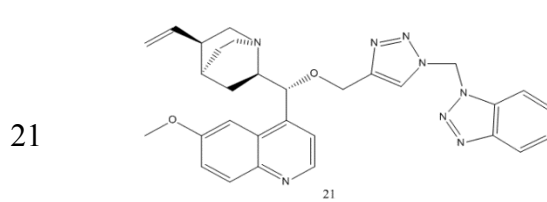
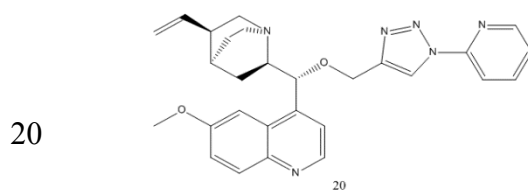
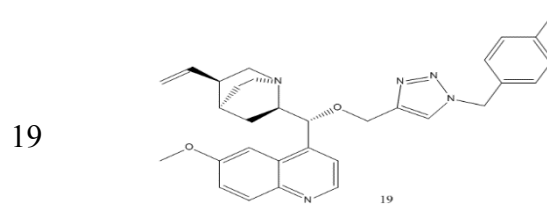
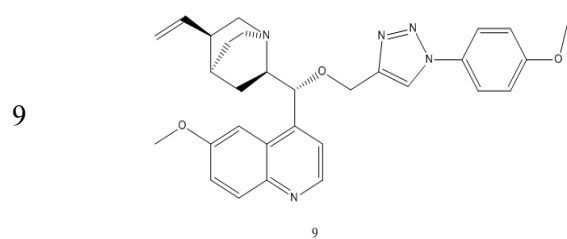
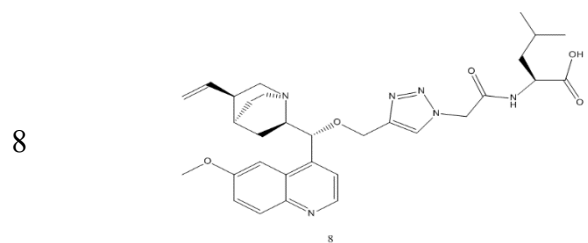
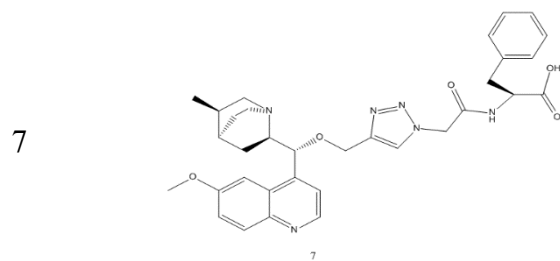
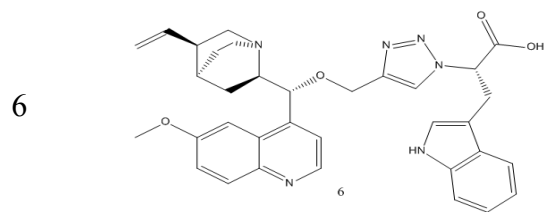
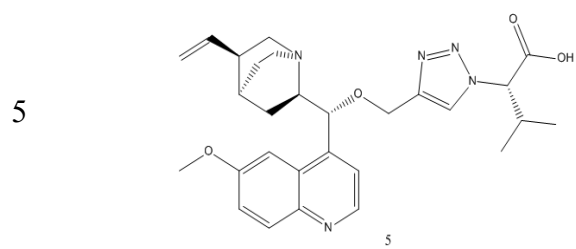
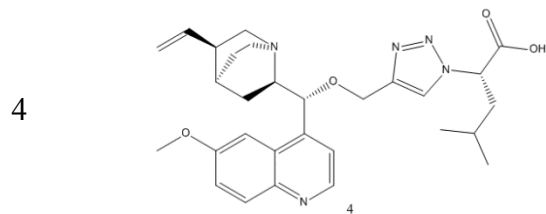
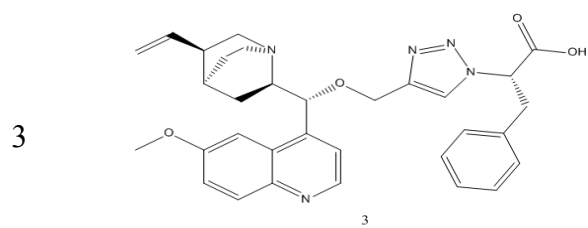
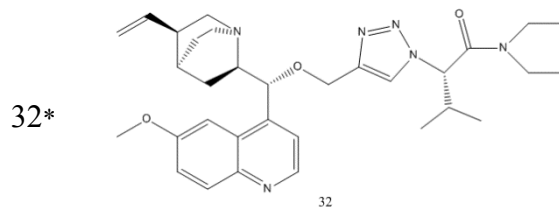
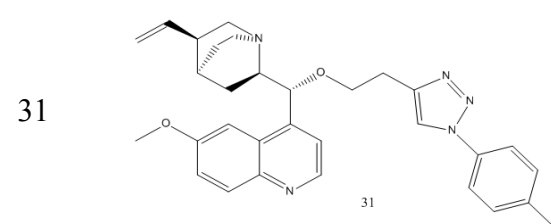
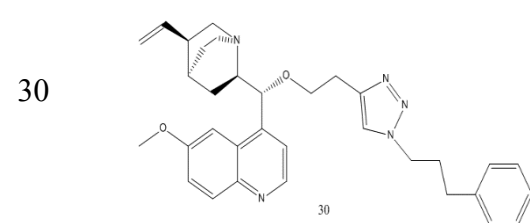
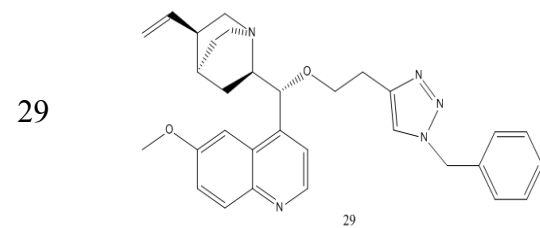
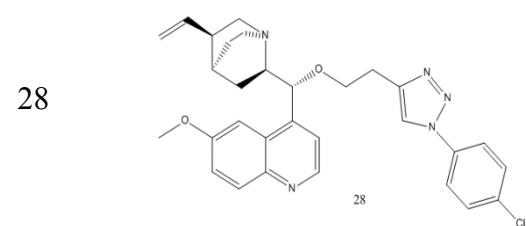
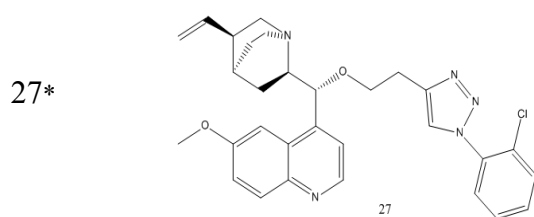
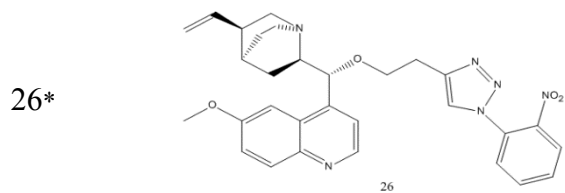
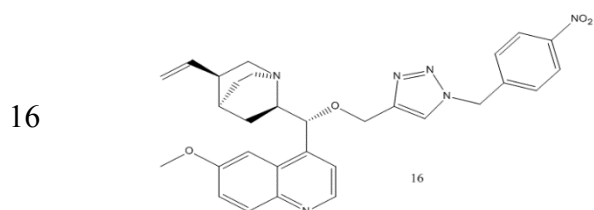
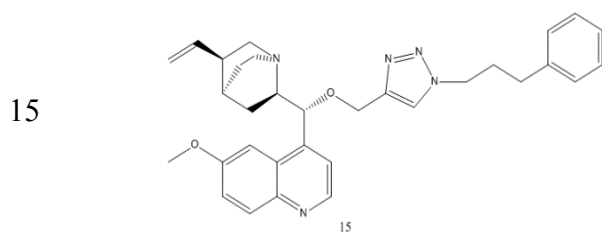
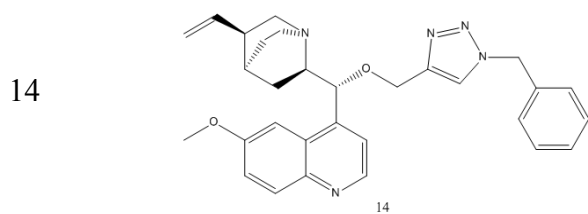
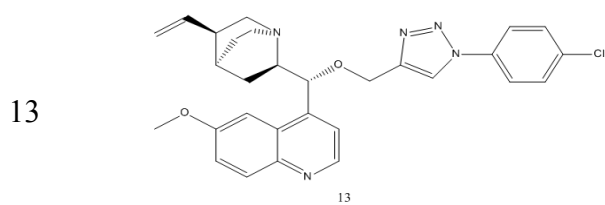
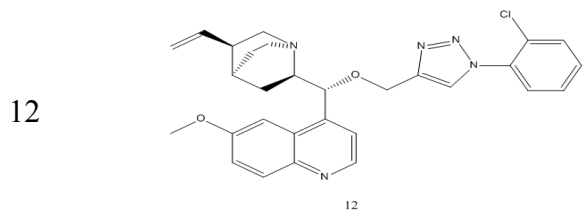
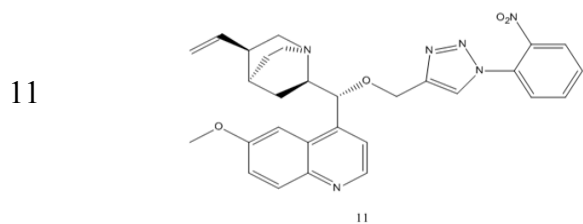
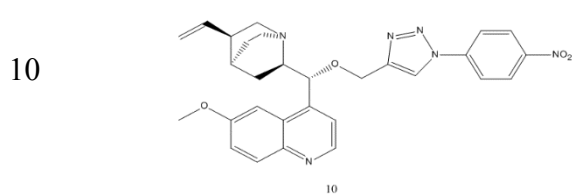


Figure 1: The chemical structure of the studied compounds

Table 1: Chemical structures of novel triazole-quinine derivatives.

N°	Compound	N°	Compound
1*		17	
2*		18	





* Test set molecules

Table2: antimalarial and predicted activities of novel triazole-quinine conjugates.

N ^o	pIC ₅₀	CoMFA		CoMSIA	
		Predicted	Residuals	Predicted	Residuals
1*	7,236	7.637	-0.401	7.52	-0.284
2*	4,387	4.632	-0.245	5.070	-0.683
3	5,113	4.771	0.342	4.837	0.276
4	4,508	4.879	-0.371	4.71	-0.202
5	4,698	5.004	-0.306	5.250	-0.552
6	5,075	4.859	0.216	5.107	-0.032
7	5,259	5.707	-0.448	4.892	0.367
8	4,920	5.694	-0.774	4.994	-0.074
9	5,657	5.808	-0.151	5.602	0.055
10	6,193	5.952	0.241	5.741	0.452
11	5,886	5.440	0.446	5.615	0.271
12	4,700	5.447	-0.747	5.543	-0.843
13	6,045	5.700	0.345	5.381	0.664
14	6,102	6.127	-0.025	5.93	0.172
15	6,050	5.579	0.471	6.226	-0.176
16	5,920	6.35	-0.43	6.371	-0.451
17	5,698	6.228	-0.53	5.793	-0.095
18	6.000	5.656	0.344	5.62	0.38
19	6,346	6.02	0.326	6.277	0.069
20	5,244	5.50	-0.256	5.592	-0.348
21	5,318	5.477	-0.159	5.618	-0.3
22	5,823	6.085	-0.262	6.037	-0.214
23	5,468	5.724	-0.256	5.296	0.172
24	7,366	7.525	-0.159	7.405	-0.039
25*	6,462	6.959	-0.497	6.388	0.074
26*	5,481	5.95	-0.469	5.939	-0.458
27*	7,431	6.747	0.684	6.954	0.477
28	7,387	7.248	0.139	7.098	0.289
29	7,397	7.347	0.05	7.182	0.215
30	7,522	7.587	-0.065	7.643	-0.121
31	7,568	7.400	0.168	7.501	0.067
32*	6,055	6.121	-0.066	5.182	0.873

* Test set molecules

2.1. Minimization and alignment

Molecular structures were sketched with sketch module in SYBYL program and optimized using the standard Tripos molecular mechanics force field [18] with Gasteiger-Hückel charges [19] by conjugated gradient method with gradient convergence criterion(0.01 kcal/mol). Simulated annealing on the optimized structures was performed with 20 cycles. The molecular alignment is the second step used to develop a performing 3D-QSAR model. Figure 2 shows the 3D structure of the core and superimposed structures of aligned data set, the data set was aligned by distill alignment technique available in SYBYL [20] using the best active compound (compound 31) as template.

2.2. 3D-QSAR Studies

To determine the contributions of electrostatic, steric, hydrophobic, bond acceptor and donor fields of the data set and to construct predictive 3D QSAR models, CoMFA and CoMSIA studies were employed relying on the molecular alignment methods. These studies were carried out as previously descriptive in the literature [21].

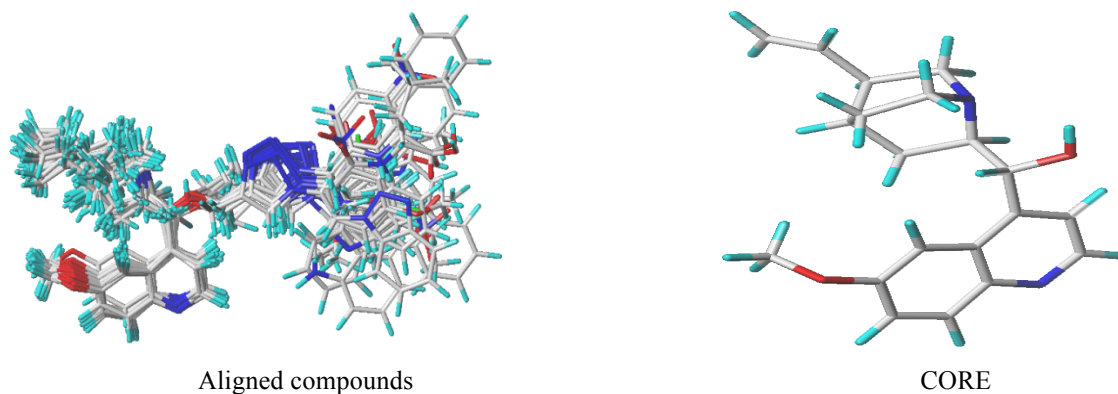


Figure 2: 3D-QSAR structure superposition and alignment of training set using molecule **31** as a template.

2.3. CoMFA studies

The CoMFA [15] model was carried out to assess steric and electrostatic energies of the Tripos force fields implemented in SYBYL-X 2.0, also attempts to establish relationships between these quantities and the measured activity. The aligned database was carried out in a three dimensional regularly with a grid spacing of 2 Å in all Cartesian directions. A carbon atom with an atomic radius of 1.52 Å and charge +1 was used as a probe to calculate the potentials, which was positioned at each lattice point of the grid box to generate, respectively, the electrostatic and steric fields, these last two, energy cut-off value was set by default at 30 kcal/mol [22].

2.4. CoMSIA studies

The CoMSIA [16] model was performed in SYBYL-X 2.0, utilizing the same grid box as employed in CoMFA computation, and the same training and test sets. Five fields' namely electrostatic, steric, hydrophobic effect and hydrogen bond acceptor and donor were calculated from analogous active molecules, to improve a CoMSIA model. For the computation of hydrogen-bond and hydrophobic potentials, a probe atom with Hydrogen bond donor or hydrogen bond acceptor of +1 and hydrophobicity +1 was used and the attenuation factor was set by default at 0.3 [23].

2.5. Partial least square (PLS) analysis

PLS method [24] employed in deriving the 3D-QSAR models is an extension of multiple regression analysis in which the original variables are superseded by a small set of their linear combinations. Moreover, in present study, the cross-validation analysis was carried out to determine the value of the cross-validation coefficient Q^2 , also optimum number of components (N) and the cross-validated standard error of predictions S_{CV} . The external validation of various models was carried out utilizing a test set of six molecules.

To get determination coefficient R^2 , the non-cross-validated analysis was carried out using the N obtained from the cross-validation analysis. The Q^2 value defines the internal predictive capability of the model, whilst R^2 value assesses the internal consistency of the model. At last, the best QSAR model was chosen relying on a combination of R^2 and Q^2 .

2.6. Y-Randomization Test

The Y-Randomization was performed [25] to validate the got models. The Y vector ($-\log IC_{50}$) is randomly shuffled several times and after every test, a new QSAR model is constructed. The new QSAR models are predictable to have low values of Q^2 and R^2 than those in the original models. Then, this technique was carried out to avoid the possibility of the chance correlation. If high values of the Q^2 and R^2 are getting, it means that an acceptable 3D-QSAR model can't be generated for this data set because of the structural redundancy and chance correlation.

2.7. Molecular Docking

Molecular docking is a technique that allows to identify of the low-energy binding modes of a small molecule (ligand) in the active site of a macromolecule (receptor). In sum, the molecular docking process commences by the algorithms posing the small ligand in a selected binding site of the target macromolecule, which can donate several conformations of the ligand. Moreover, the interactions between the ligand and the macromolecule are assessed with scoring functions to estimate the binding energy and finally identify the optimal binding mode [26].

In present study, this technique was carried out using Surflex-dock available in SYBYL-X.2.0. This latter was performed for the preparation steps of proteins and ligands for the docking protocol. Furthermore, Discovery Studio 2016 [27] and PyMol [28] software's were carried out to analyze the obtained results.

2.7.1. Macromolecule preparation

The antimalarial protein was downloaded from the Protein Data Bank (<http://www.rcsb.org>), (PDB entry code: 1J3K) [29]. The ligand was extracted then the most and the less active ligands (compounds 31 and 2) from our data set were docked in the active site of the studied enzyme. Moreover, Discovery Studio 2016 is used to prepare the PDB file [28]. Then solvent molecules and cofactors were extracted from the model.

2.7.2. Ligand preparation

For docking study, the 3D structures of ligands (compounds 31 and 2) were constructed using the SKETCH option in SYBYL. Moreover; they were minimized under the Tripos standard force field [18] with Gasteiger-Hückel charges [19] by conjugated gradient method with gradient convergence criterion of 0.01 kcal/mol Å in SYBYL software.

3. Results and discussion

3.1. CoMFA results

PLS summary shows that CoMFA model has high R^2 (0.98) and F (229.904) values, small estimation error Scv (0.149), the cross-validated determination coefficient Q^2 (0.61) with four optimum number of components. The external predictive ability of QSAR model is usually cross checked and validated using test sets. The six randomly selected test sets-were optimized and aligned in the same manner as training sets. The external validation gave high value of R_{test}^2 (0.92) indicating that prediction ability of CoMFA model is acceptable. Moreover the ratios of steric and electrostatic contributions were found to be 58:42 which indicate that steric interactions are much more important than electrostatic.

3.2. CoMSIA results

To explain and predict quantitatively the electrostatic, steric, hydrophobic, donor bond and acceptor fields effects of substituents on antimalarial activity of 32 compounds. A 3D-QSAR model was proposed based on CoMSIA descriptor.

Different combinations of five fields were generated. The best CoMSIA proposed model contains mainly four fields (Electrostatic, donor and Acceptor, Hydrophobic). Table 2 indicate that CoMSIA developed model has high Cross and non-cross validated correlation coefficients with Q^2 (0.76) and R^2 (0.95) respectively, The F test value (95.894) values, Standard error estimation obtained has a low value 0.228 and optimal number of principal components is two, which is reasonable considering the number of molecules used to build the model.

Finally, the prediction ability of the proposed model is confirmed by using the external validation, the R_{test}^2 value obtained is 0.85. These statistics results demonstrated the good stability and the powerful predictive capability of CoMSIA model.

Table 3: PLS Statistics of CoMFA and CoMSIA models

Model	Q ²	R ²	Scv	F	N	Fractions					
						Rtest ²	Ster	Elec	Acc	Don	Hyd
CoMFA	0.61	0.98	0.149	229.904	4	0.92	0.578	0.422	-	-	-
CoMSIA	0.76	0.95	0.228	95.894	2	0.85	0.063	0.253	0.269	0.198	0.217

R²: Non-cross- validated determination coefficient

Q²: Cross-validated determination coefficient

N: Optimum number of components

F: F-test value

Scv: Standard error of the estimate.

Rtest²: External validation determination coefficient

The correlations of predicted and observed pIC_{50} values are displayed in figure 3.

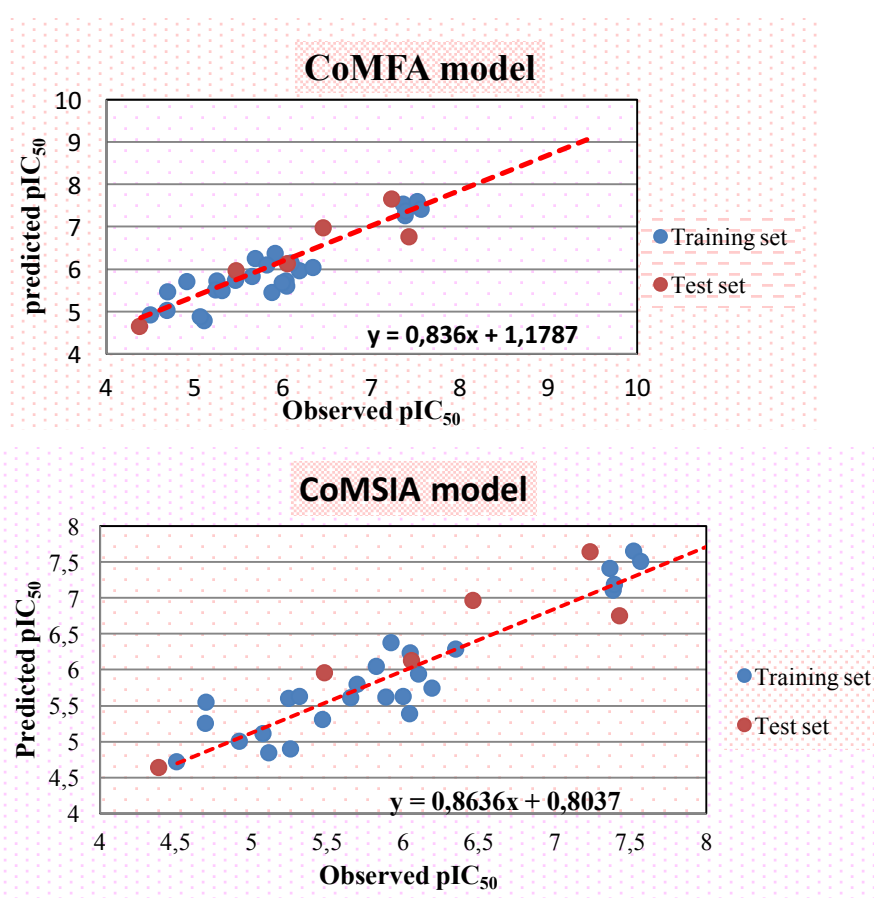


Figure 3: Experimental versus predicted activity of the training and test set relying on the CoMFA and CoMSIA model.

According to the figure 3 we notice a regular distribution of activity values depending on the experimental values. Moreover, the determination coefficient R² and Rtest² of CoMFA Model is higher than CoMSIA's; while Q² is lower. And about the value of the standard error, we notice that CoMFA model has a high Scv than CoMSIA's model that is showed in Figure 3.

3.3. Graphical Interpretation of CoMFA and CoMSIA results

CoMFA and CoMSIA contour maps were produced to streamline regions where the activity can be decreased or increased. CoMFA contours are illustrated in figure 4 (a, b), while CoMSIA contours are

displayed in figure 5 (a, b, c, d, e), in this study, compound 31 was used as a reference structure.

3.4. CoMFA Contour Maps

CoMFA steric interactions are showed with green and yellow colors (figure 4.a); while electrostatic interactions are showed with red and blue colored contours (figure 4.b). The bulky substituents are favored around green regions, while yellow regions bulky substituents are unflavored. Moreover, the blue regions indicate that nucleophilic groups are favored, while, and in the red regions are unflavored.

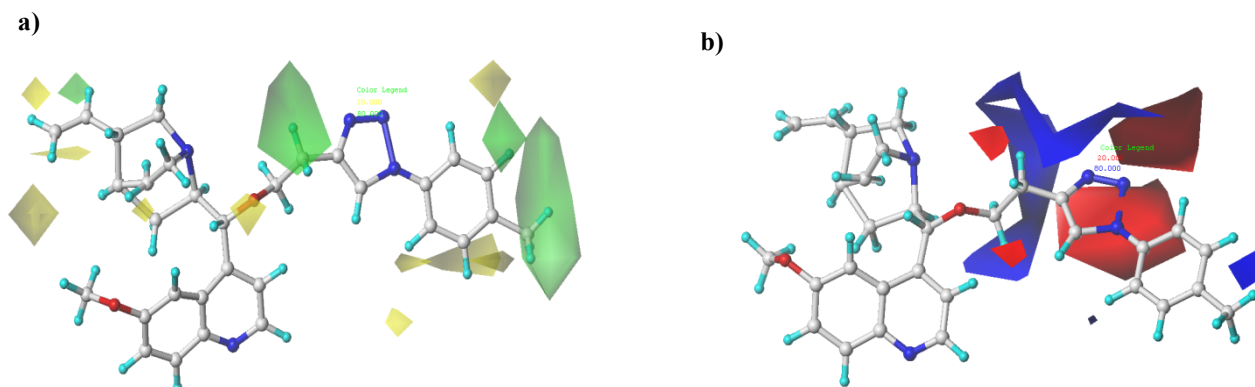


Figure 4: Std* coeff. Contour maps of CoMFA analysis with 2 Å grids spacing in combination with compound **31**. **a)** Steric fields: yellow contours (20% contribution) show regions where voluminous groups are required to decrease the activity, while green contours (80% contribution) show regions where voluminous groups are required to increase the activity. **b)** Electrostatic fields: red contours (20% contribution) show regions where groups with negative charges increase activity, while blue contours (80% contribution) show regions where groups with positive charges increase activity.

The figure 4 shows, that bulky groups with electro-donating character around the methyl of phenyl can increase the activity of the compounds. This result can explain the high activity of some compounds in the data set such as compound 24 ($pIC_{50} = 7.36$), compound 29 ($pIC_{50} = 7.39$) and compound 30 ($pIC_{50} = 7.52$) that have an electro-donating bulky groups.

Moreover, the bulky groups with electro-donating character near to position 4 of 1.2.3 triazolic cycle can increase the activity. And using groups with electro-attracting character near of this position can also increase the activity. Besides, groups with electro-attracting character around 1.2.3 triazolic cycle would improve the activity.

In addition, green contour around *meta* position of phenyl indicate that bulky group in this position can increase the activity.

3.5. CoMSIA Contour Map

Green contours around *ortho* and *meta* positions of phenyl group indicate that bulky groups in these positions can increase the activity. While yellow contour around *ortho*, *meta* positions of phenyl and hydrogen atom of 1.2.3 triazolic cycle explain why compounds with small substitutions in these positions have a high activities (figure 5a).

Bleu contour near to position 4 of 1.2.3 triazolic cycle means that the substitution with electron-donating groups would increase the activity. While red contours around the 1.2.3 triazolic cycle can decrease the activity (figure 5b).

Yellow contour around *meta* and *para* positions of phenyl indicate that hydrophobic groups may increase the activity, while the white contour around *ortho* position of phenyl and near the 1.2.3 triazolic cycle indicates that hydrophilic groups are favored (figure 5c).

Magenta contour around oxygen atom, positions 3, 4 of 1.2.3 triazolic cycle and position near to position 4 of this group explain that substituent with hydrogen bond acceptor character can increase the activity. Whereas, red contour cover hydrogen atom exposed the importance of the hydrogen bond donor group (figure 5d).

Cyan contour around *ortho*, *meta* and *para* positions of phenyl group indicates that substituent with hydrogen bond donor character in these positions would improve the activity (figure 5e). These results explain very well the high activity obtained of compound 31 which has hydrophobic groups (CH₃) in *para* position of phenyl.

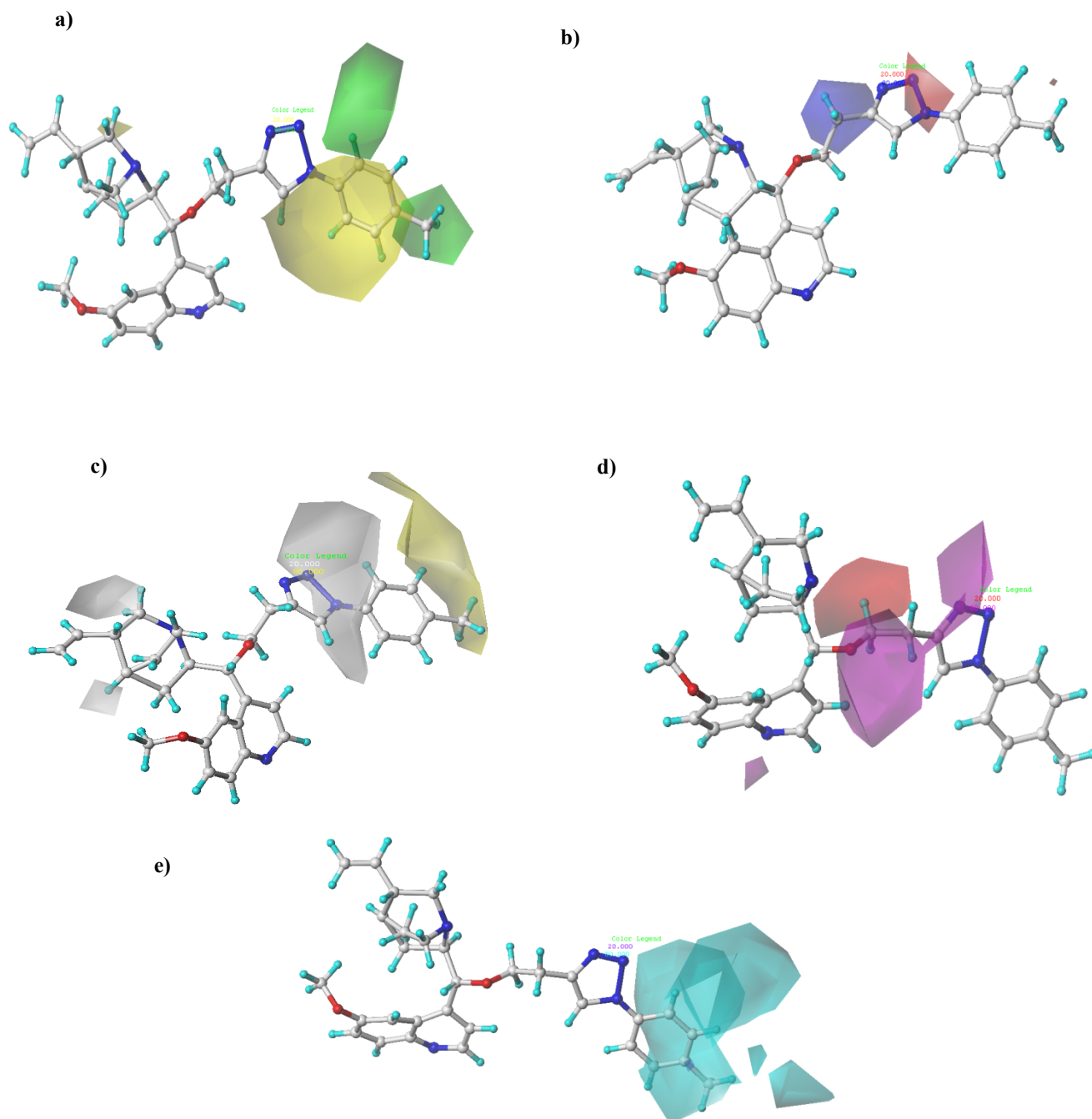


Figure 5: Contour maps of CoMSIA analysis with 2 Å grids spacing in combination with compound 31. **a)** steric fields: yellow contours (20% contribution) designate regions where huge groups decrease activity, whereas green contours (80% contribution) designate regions where huge groups improve the activity, **b)** Electrostatic fields: red contours (20% contribution) demonstration regions where electron-withdrawing groups growth activity; blue contours (80% contribution) demonstration regions where electron- withdrawing groups reduce activity, **c)** Hydrophobic fields: white contours (20% contribution) designate hydrophobic groups are unfavorable, whereas yellow contours (80% contribution) demonstration hydrophobic groups are preferred, **d)** H-bond acceptor fields: Magenta contours (80% contribution) show regions where an H-bond acceptor substituents improve the activity, red contours (20% contribution) designate regions where H-bond acceptor substituents reduce the activity. **e)** H- bond donor fields: Cyan contours (80% contribution) show regions where H-bond donor substituents growth activity while purple contours (20% contribution) show regions where H-bond donor substituents reduce the potency.

3.6. Y-Randomization

To affirm the CoMSIA and CoMFA models, the Y-Randomization method is executed. Divers random shuffles of the dependent variable were carried out then after every shuffle, a 3D-QSAR was developed and the obtained results are illustrated in Table 4. The feeble Q^2 and R^2 values obtained after every shuffle showed that the good result in our original CoMFA and CoMSIA models are not due to a chance correlation of the training set.

Table 4: Q^2 and R^2 values after random Y-randomization tests

Iteration	CoMFA		CoMSIA	
	Q^2	R^2	Q^2	R^2
1	-0.07	0.88	0.21	0.77
2	0.009	0.95	0.28	0.88
3	-0.19	0.91	-0.005	0.85
4	0.06	0.95	-0.34	0.78
5	-0.78	0.97	-0.45	0.77
6	0.22	0.98	0.12	0.87

3.7. New designed molecules

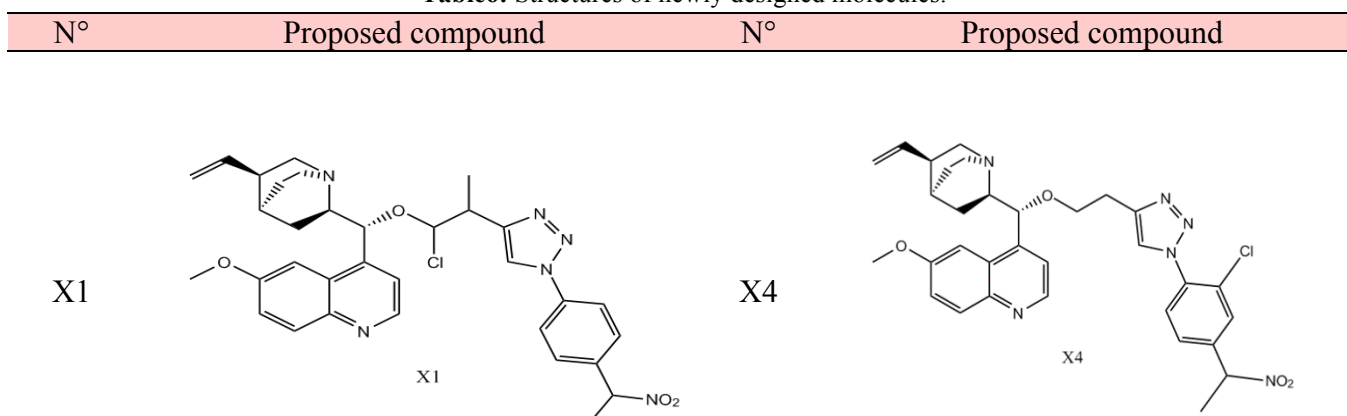
Relying on the proposed 3D-QSAR (CoMFA/CoMSIA) models, five new triazoles analogues were designed (Table 5). The new predicted structure X1 shows higher activity ($pIC_{50} = 7.923$ for CoMSIA) than compound 31 that's the most active compound of the series (table 6).

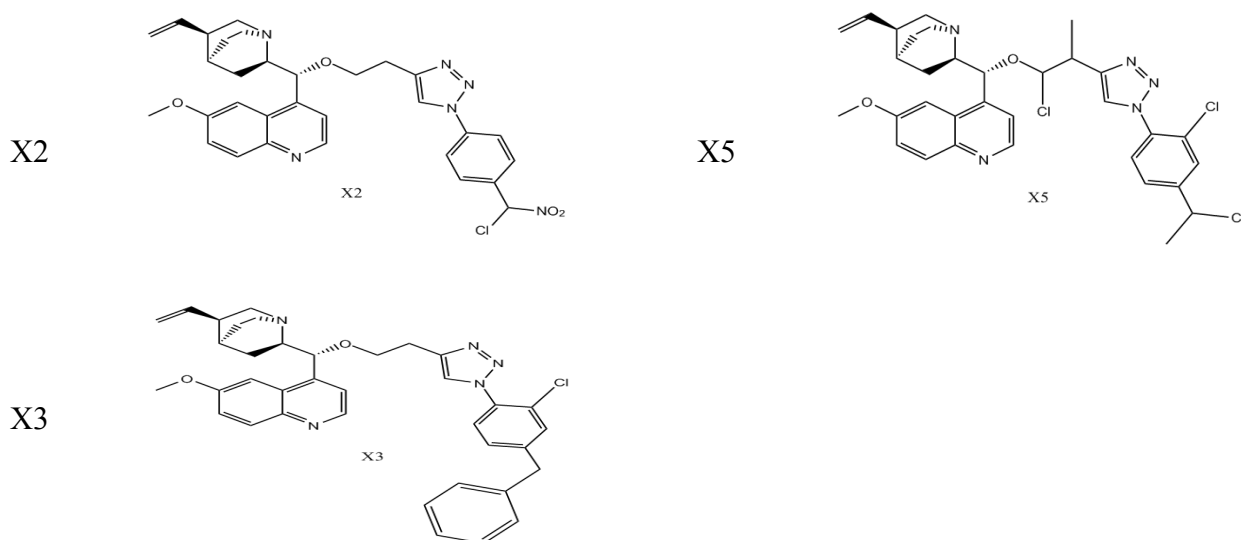
Moreover, these newly molecules were minimized and aligned to the database using compound 31.

Table 5: Predicted pIC_{50} of newly designed compounds based on CoMFA and CoMSIA 3D-QSAR models.

N°	Predicted pIC_{50}	
	CoMFA	CoMSIA
X1	7.141	7.923
X2	7.329	7.879
X3	7.312	7.860
X4	7.340	7.845
X5	7.148	7.756

Table6: Structures of newly designed molecules.





3.7. Docking results

Surflex-dock was applied to expound the activity of the compounds, and its relation with the interactions between the active molecule (compound 31), the inactive molecule (compound 2) and the proposed molecule (compound X1) with receptor (PDB ID: 1J3K)

According to **figure 6**, the active compound (compound 31) presents a pi-Alkyl interaction with LEU A:119, ILE A:112, PHE A:58, MET A:55 residues around R group explain the high activity of compound 31, and it is according to CoMSIA contour maps analysis, pi-Lone Pair with ASN A:108 residue, pi-sigma interaction with VAL A:195 residue, conventional hydrogen bond interaction with LEU A:46 residue, pi-donor hydrogen bond interaction with LEU A:40, SER A:111, GLY A:166 residues. While the inactive compound (compound 2) **figure 7**, presents, pi-donor hydrogen bond with SER A:111, ASN A:108, THR A:107, VAL A:45, GLY A:44 residues, pi-Alkyl interaction with MET A:55, PHE A:58, VAL A:195, ILE A:112, LEU A:46 residues. Which means that group R in compound 31 (the active compound) presents a lot of hydrogen bond than compound 2(the inactive compound).

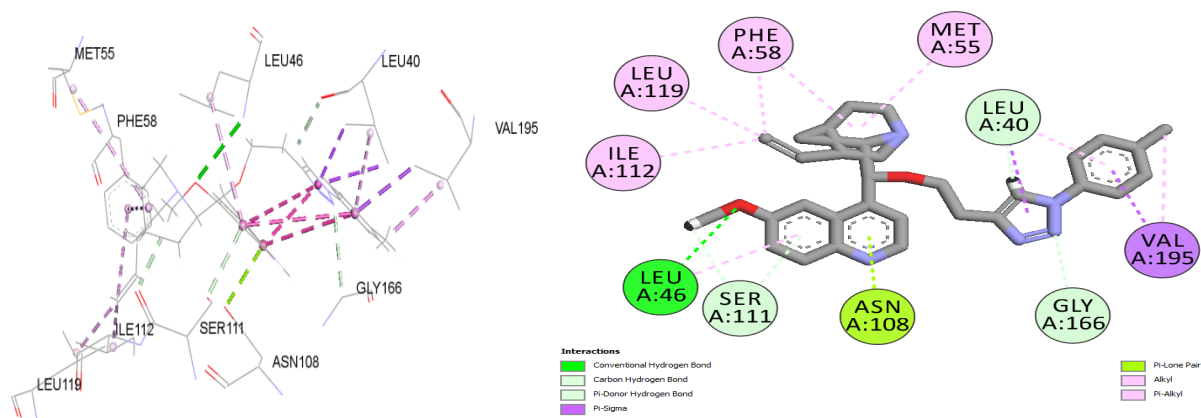


Figure 6: Docking interactions between the protein 1J3K and the compound 31 as the active compound in database.

Furthermore, the proposed X1 compound **figure 8** shows pi-Alkyl interaction with ALA A:16, LEU A:40, ILE A:112, LEU A:46, PHE A:58, LEU A:119, VAL A:195, MET A:55, ARG A:59 residues, carbon hydrogen bond interaction with ASP A:54, VAL A:45, ASN A:108, SER A:111 residues, pi-pi T-shaped with PHE A:116 residue, and conventional hydrogen bond interaction with TYR A:170 residue, these interactions explain the stability and the high activity of the proposed compound.

The **figure 9** shows the green color around R group designate the regions where H-bond acceptor is preferred, whereas the brown color around R1 shows where hydrophobic groups are preferred. In conclusion all these results have been used for the design of new molecules with high antimalarial activity against the malaria.

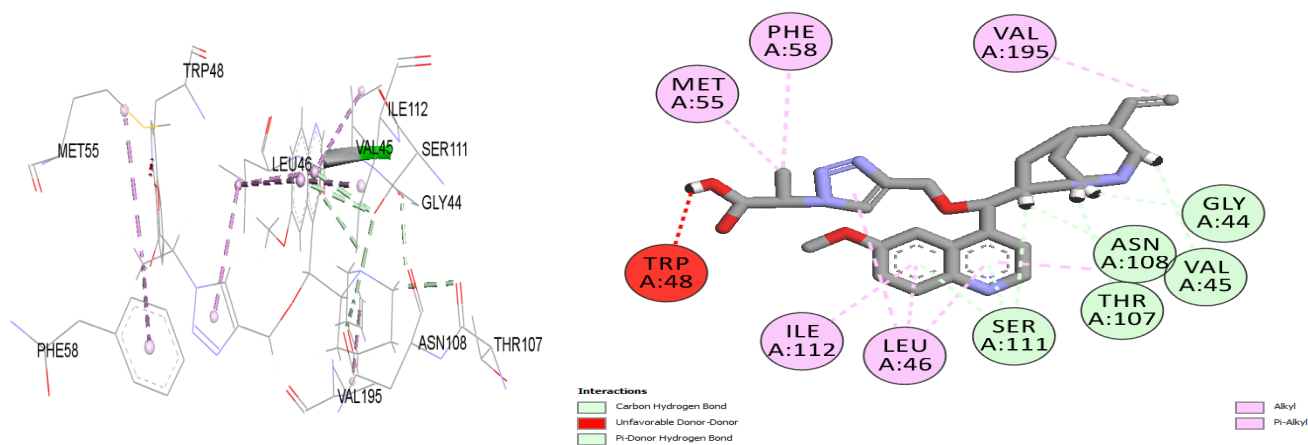


Figure 7: Docking interactions between the protein **1J3K** and the compound **2** as the inactive compound in database.

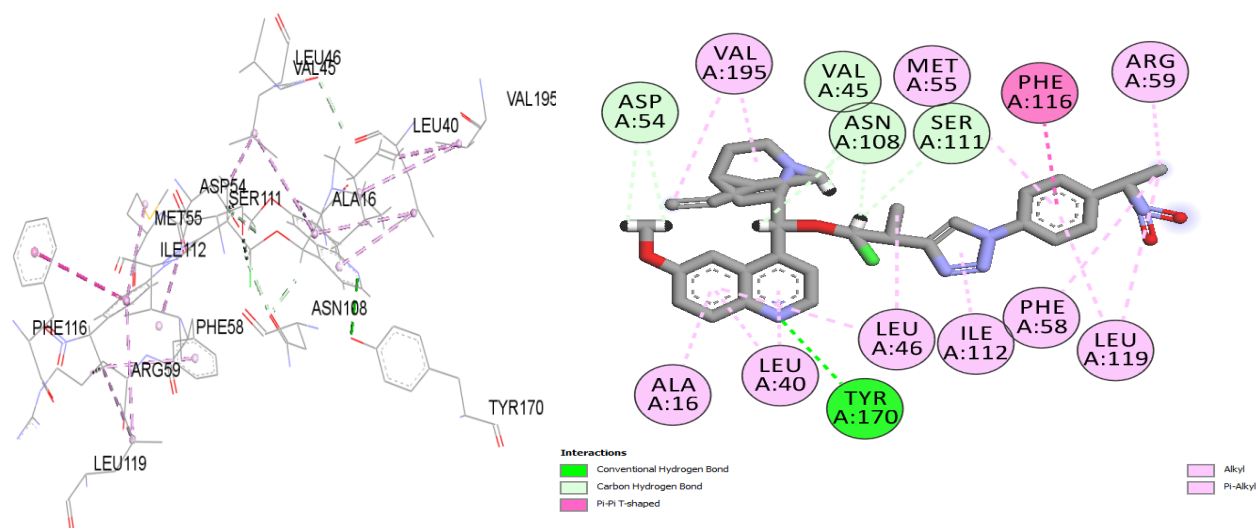


Figure 8: Docking interactions between the protein and the proposed compound **X1**.

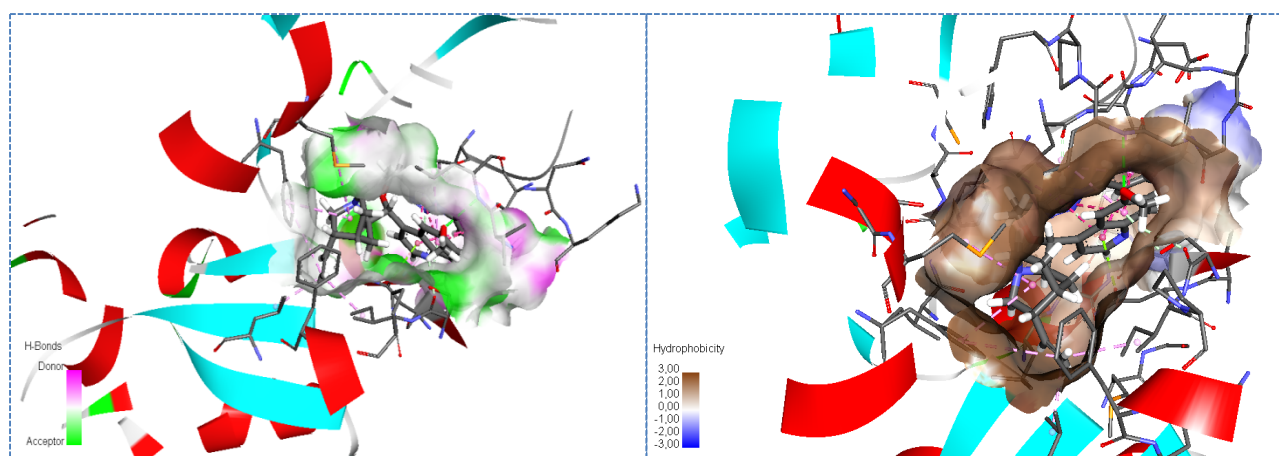


Figure 9: The interaction H-bond and Hydrophobicity between the compound **31** (active molecule) and the protein **1J3K**, visualized with Discovery studio visualizer program.

Conclusion

In conclusion, the present study shows an excellent results of 3D-QSAR model using CoMFA ($Q^2=0.61$, $R^2=0.98$) and CoMSIA ($Q^2=0.76$, $R^2=0.95$) models that produce equally good models in term of several rigorous statistical keys, such as Q^2 and $Rtest^2$, for both the internal and external data sets. 3D-QSAR employed to explore the structure-activity relationship of novel triazole-quinine derivatives as antimalarial agents. Besides, CoMFA and CoMSIA contours results provided ample information to comprehend the structure-activity relationship and identify structural features influencing the activity. Based on their contours maps new triazoles-quinine was proposed with high antimalarial activity. Meanwhile, molecular docking confirmed the stability of high and low active compounds and also the new proposed ones by interpreting interactions between these compounds and antimalarial receptor. So this results show that the large difference between the least and most compounds, this is due to lack of halogen interactions in the case of the compound inactive, which affirms CoMFA and CoMSIA results.

Acknowledgments- we are grateful to the “Association Marocaine des Chimistes Théoriciens” (AMCT) for its pertinent help concerning the programs.

References

1. World-malaria-report-2017.<http://www.who.int/malaria/publications/world-malaria-report-2017/en/>.
2. P. Shetty, The Numbers game, *Nature*, 484, 26 April (2012) S14-S15.
3. Centers for Disease Control and Prevention. The history of malaria, An Ancient Disease (accessed October. 6, 2011).
4. World Health Organization. Malaria. (Accessed October. 6, 2011).
5. W. H. Organization, Guidelines for the Treatment of Malaria, W.H.O, 2006.
6. Y-K. Zhang, J.J. Plattner, E.E. Easom, R.T. Jacobs, et all, Benzoxaborole Antimalarial Agents, *J. Med. Chem.* 60 (2017) 5889- 5908.
7. P. W. Gething , A. P. Patil , D. L. Smith , C. A. Guerra , I. RF Elyazar , G. L. Johnston, A. J .Tatem and S. I. Hay, A new world malaria map: Plasmodium falciparum endemicity in 2010,*Malaria .J.* 10 (2011) 1475-2875.
8. K.E. Battle, P.W. Gething, I.R.F. Elyazar, C.L. Moyes, M.E. Sinka, R.E. Howes, C.A. Guerra, R.N. Price, J.K. Baird, S.I. Hay, in: R.P.S.I. Hay, J.K. Baird (Eds.), *Advances in Parasitology.* 80 (2012) 1-111.
9. T. Wu, A.S. Nagle and A.K. Chatterjee, Malaria Parasites, *Curr Med Chem.* 18(6) (2011) 853-871.
10. T. Sreekanth, Y. Rajeshwar, *J. Current Protein & Peptide Science.* 17 (2016) 275-279.
11. B.S. Crabb, J.G. Beeson, R. Amino, R. Menard, A. Waters, E.A. Winzeler, M. Wahlgren, D.A. Fidock, S. Nwaka, *Nature* 484 (7395) (2012) S22-S23.
12. J.K. Baird, Effectiveness of Antimalarial Drugs, *the New England Journal of Medicine.* 352 (2005) 1565-1577.
13. X-M. Chu, C. Wang, W. L. Wang, L.L. Liang, W. Liu, K.K. Gong, K. Sun, Triazole derivatives and their antiplasmodial and antimalarial activities, *Eur. J. Med. Chem.* 166 (2019) 206-223.
14. Y. Fukunishi, S. Yamasaki, I. Yasumatsu, K. Takeuchi, T. Kurosawa, and H. Nakamura, Quantitative Structure-activity Relationship (QSAR) Models for Docking Score Correction, *J. mol inform.* 36 (1-2) (2017) 1600013.
15. R. D. Cramer III, D. E. Patterson and J. D. Bunce. Comparative molecular field analysis (CoMFA). *J. Am. Chem. Soc.* 110 (1988) 5959-5967.
16. G. Klebe, U. Abraham, and T. Mietzner. Comparative Molecular similarity index analysis (CoMSIA) of drug molecules to correlate and predict their biological activity. *J. Med. Chem.* 37 (1994) 4130-4146.

17. H. M. Faidallah, Siva S. Panda, Juan C. Serrano et al, *J. Bioorg Med Chem.* 24 (2016) 3527-3539.
18. M. Clark, R. D. Cramer, and N. V. Opdenbosch, General purpose tripos 5.2 force field, *J. Comp. Chem.* 10(8) (1989) 982-1012
19. W. P. Purcell and J. A. Singer, A brief review and table of semi empirical parameters used in the HMO method, *J.Chem.Engineer. data.* 12 (2) (1967)235–246.
20. Tripos Inc., St. Louis, MO, USA, SYBYL-X 2.0, (n.d.). <http://www.tripos.com>
21. A. Aouidate, A. Ghaleb, et al, molecular docking and Furanone derivatives as new inhibitors of CDC7 kinase: development of structure activity relationship model using 3D-QSAR, and in silico ADMET. *J. Struc. Chem.* 29 (2018) 1031-1043.
22. L. Stähle, S. Wold, Experimental design in biomedical research and multivariate data analysis. *Prog.Med.Chem.*25 (1988) 291–338.
23. J. Zheng, G. Xiao, J. Guo, Y. Zheng, H. Gao, S. Zhao, K. Zhang, P. Sun, Exploring QSARs for 5-Lipoxygenase (5-LO) Inhibitory Activity of 2-Substituted 5-Hydroxyindole-3- Carboxylates by CoMFA and CoMSIA, *Chem. Biol. Drug Des.* 78 (2011) 314–321.
24. S. Wold, *Quant, Struct. Act. Relat.* 10 (1991) 191.
25. C. Rücker, G. Rücker, M. Meringer, Y-randomization and its variants in QSPR/QSAR, *J.Chem. Inf. Model.* 47 (2007) 2345–2357.
26. A. Aouidate, A. Ghaleb, M. Ghamali, A. Ousaa, M. Choukrad, A. Sbai, M. Bouachrine, T. Lakhliifi, 3D- QSAR studies, molecular docking and ADMET evaluation, using thiazolidine derivatives as template to obtain new inhibitors of PIM1 kinase, *J. Comp. Biol. Chem.* 74 (2018) 201-211
27. Dassault Systèmes BIOVIA, Discovery Studio Modeling Environment, Release 2017, San Diego: Dassault Systèmes., (2016). <http://accelrys.com/products/collaborative-science/bioviadiscovery-studio/> (accessed February 25, 2017).
28. W. DeLano, The PyMOL Molecular Graphics System DeLano Scientific, Palo Alto, CA, USA, (2002). <http://www.pymol.org> (accessed February 25, 2017).
29. X. Qiu, C.A. Janson, W.W. Smith, S.M. Green, P. McDevitt, K. Johanson, P. Carter, M. Hibbs, C. Lewis, A. Chalker, A. Fosberry, J. Lalonde, J. Berge, P. Brown, C.S.V. Houge-Frydrych, R.L. Jarvest, Crystal structure of *Staphylococcus aureus* tyrosyl-tRNA synthetase in complex with a class of potent and specific inhibitors, *Protein Science.* 10 (n.d.) 2008–2016.

(2020) ; <http://www.jmaterenvirosci.com/>